Level-crossing and modal structure in microdroplet resonators

Sarah T. Attar,[1,*] Vladimir Shuvayev,[2] Lev Deych,[2,3] Leopoldo L. Martin,[1] and Tal Carmon[1]

[1]*Department of Mechanical Engineering, Technion-Israel Institute of Technology, 3200003 Haifa, Israel*
[2]*Physics Department, Queens College of CUNY, Flushing, NY 11367, USA*
[3]*The Graduate Center of CUNY, 365 5th Ave, New York, NY 10016, USA*
[*]*stattar@tx.technion.ac.il*

Abstract: We fabricate a liquid-core liquid-clad microcavity that is coupled to a standard tapered fiber, and then experimentally map the whispering-gallery modes of this droplet resonator. The shape of our resonator is similar to a thin prolate spheroid, which makes space for many high-order transverse modes, suggesting that some of them will share the same resonance frequency. Indeed, we experimentally observe that more than half of the droplet's modes have a sibling having the same frequency (to within linewidth) and therefore exhibiting a standing interference-pattern.

©2016 Optical Society of America

OCIS codes: (140.4780) Optical resonators; (140.3945) Microcavities.

References and links

1. A. B. Matsko and V. S. Ilchenko, "Optical resonators with whispering gallery modes I: basics," IEEE J. Sel. Top. Quantum Electron. **12**(1), 3–14 (2006).
2. V. Braginsky, M. Gorodetsky, and V. Ilchenko, "Quality-factor and nonlinear properties of optical whispering-gallery modes," Phys. Lett. A **137**(7-8), 393–397 (1989).
3. D. K. Armani, T. J. Kippenberg, S. M. Spillane, and K. J. Vahala, "Ultra-high-Q toroid microcavity on a chip," Nature **421**(6926), 925–928 (2003).
4. Y. Yang, J. Ward, and S. N. Chormaic, "Quasi-droplet microbubbles for high resolution sensing applications," Opt. Express **22**(6), 6881–6898 (2014).
5. F. Vollmer, S. Arnold, and D. Keng, "Single virus detection from the reactive shift of a whispering-gallery mode," Proc. Natl. Acad. Sci. U.S.A. **105**(52), 20701–20704 (2008).
6. T. Lu, H. Lee, T. Chen, S. Herchak, J.-H. Kim, S. E. Fraser, R. C. Flagan, and K. Vahala, "High sensitivity nanoparticle detection using optical microcavities," Proc. Natl. Acad. Sci. U.S.A. **108**(15), 5976–5979 (2011).
7. A. Ashkin and J. Dziedzic, "Observation of resonances in the radiation pressure on dielectric spheres," Phys. Rev. Lett. **38**(23), 1351–1354 (1977).
8. J. B. Snow, S.-X. Qian, and R. K. Chang, "Stimulated Raman scattering from individual water and ethanol droplets at morphology-dependent resonances," Opt. Lett. **10**(1), 37–39 (1985).
9. A. Jonáš, Y. Karadag, M. Mestre, and A. Kiraz, "Probing of ultrahigh optical Q-factors of individual liquid microdroplets on superhydrophobic surfaces using tapered optical fiber waveguides," J. Opt. Soc. Am. B **29**(12), 3240–3247 (2012).
10. S. Avino, A. Krause, R. Zullo, A. Giorgini, P. Malara, P. De Natale, H. P. Loock, and G. Gagliardi, "Direct Sensing in Liquids Using Whispering-Gallery-Mode Droplet Resonators," Adv. Opt. Mater. **2**(12), 1155–1159 (2014).
11. S. Maayani, L. L. Martin, S. Kaminski, and T. Carmon, "Cavity Optocapillaries," Optica **3**(5), 552 (2016).
12. S. Maayani, L. L. Martin, and T. Carmon, "Water-walled microfluidics for high-optical finesse cavities," Nat. Commun. **7**, 10435 (2016).
13. R. Dahan, L. L. Martin, and T. Carmon, "Droplet optomechanics," Optica **3**(2), 175–178 (2016).
14. M. Hossein-Zadeh and K. J. Vahala, "Fiber-taper coupling to Whispering-Gallery modes of fluidic resonators embedded in a liquid medium," Opt. Express **14**(22), 10800–10810 (2006).
15. Y. Fainman, L. P. Lee, D. Psaltis, and C. Yang, *Optofluidics: Fundamentals, Devices, and Applications* ((McGraw-Hill New York: 2010)).
16. S. Kaminski, L. L. Martin, and T. Carmon, "Tweezers controlled resonator," Opt. Express **23**(22), 28914–28919 (2015).
17. F. Vollmer, D. Braun, A. Libchaber, M. Khoshsima, I. Teraoka, and S. Arnold, "Protein detection by optical shift of a resonant microcavity," Appl. Phys. Lett. **80**(21), 4057–4059 (2002).

18. S. Arnold, M. Khoshsima, I. Teraoka, S. Holler, and F. Vollmer, "Shift of whispering-gallery modes in microspheres by protein adsorption," Opt. Lett. **28**(4), 272–274 (2003).
19. A. Mazzei, S. Götzinger, L. S. Menezes, G. Zumofen, O. Benson, and V. Sandoghdar, "Controlled coupling of counterpropagating whispering-gallery modes by a single Rayleigh scatterer: a classical problem in a quantum optical light," Phys. Rev. Lett. **99**(17), 173603 (2007).
20. S. I. Shopova, R. Rajmangal, Y. Nishida, and S. Arnold, "Ultrasensitive nanoparticle detection using a portable whispering gallery mode biosensor driven by a periodically poled lithium-niobate frequency doubled distributed feedback laser," Rev. Sci. Instrum. **81**(10), 103110 (2010).
21. L. He, Ş. K. Özdemir, J. Zhu, W. Kim, and L. Yang, "Detecting single viruses and nanoparticles using whispering gallery microlasers," Nat. Nanotechnol. **6**(7), 428–432 (2011).
22. S. Shopova, R. Rajmangal, S. Holler, and S. Arnold, "Plasmonic enhancement of a whispering-gallery-mode biosensor for single nanoparticle detection," Appl. Phys. Lett. **98**(24), 243104 (2011).
23. D. Keng, X. Tan, and S. Arnold, "Whispering gallery micro-global positioning system for nanoparticle sizing in real time," Appl. Phys. Lett. **105**(7), 071105 (2014).
24. A. Savchenkov, A. Matsko, V. Ilchenko, D. Strekalov, and L. Maleki, "Direct observation of stopped light in a whispering-gallery-mode microresonator," Phys. Rev. A **76**(2), 023816 (2007).
25. T. Carmon, H. G. Schwefel, L. Yang, M. Oxborrow, A. D. Stone, and K. J. Vahala, "Static envelope patterns in composite resonances generated by level crossing in optical toroidal microcavities," Phys. Rev. Lett. **100**(10), 103905 (2008).
26. S. Maayani, L. L. Martin, S. Kaminski, and T. Carmon, "Cavity Optocapillaries," arXiv preprint arXiv:1512.07741 (2015).
27. S. Kaminski, L. L. Martin, S. Maayani, and T. Carmon, "Ripplon Laser," arXiv preprint arXiv:1603.02218 (2016).
28. L. Deych and V. Shuvayev, "Theory of nanoparticle-induced frequency shifts of whispering-gallery-mode resonances in spheroidal optical resonators," Phys. Rev. A **92**(1), 013842 (2015).
29. L. Deych and J. Rubin, "Rayleigh scattering of whispering gallery modes of microspheres due to a single dipole scatterer," Phys. Rev. A **80**(6), 061805 (2009).
30. J. Zhu, S. K. Ozdemir, Y.-F. Xiao, L. Li, L. He, D.-R. Chen, and L. Yang, "On-chip single nanoparticle detection and sizing by mode splitting in an ultrahigh-Q microresonator," Nat. Photonics **4**(1), 46–49 (2010).
31. S. Ozdemir, L. He, J. Zhu, F. Monifi, W. Kim, O. Kenechukwu, H. Yilmaz, S. Huang, and L. Yang, "On-chip whispering-gallery-mode microlasers and their applications for nanoparticle sensing," in *SPIE OPTO*, (International Society for Optics and Photonics, 2013), 86270N–86270N–86210.
32. J. C. Knight, G. Cheung, F. Jacques, and T. A. Birks, "Phase-matched excitation of whispering-gallery-mode resonances by a fiber taper," Opt. Lett. **22**(15), 1129–1131 (1997).
33. M. Cai, O. Painter, and K. J. Vahala, "Observation of critical coupling in a fiber taper to a silica-microsphere whispering-gallery mode system," Phys. Rev. Lett. **85**(1), 74–77 (2000).
34. S. M. Spillane, T. J. Kippenberg, O. J. Painter, and K. J. Vahala, "Ideality in a fiber-taper-coupled microresonator system for application to cavity quantum electrodynamics," Phys. Rev. Lett. **91**(4), 043902 (2003).
35. T. Carmon, S. Y. Wang, E. P. Ostby, and K. J. Vahala, "Wavelength-independent coupler from fiber to an on-chip cavity, demonstrated over an 850nm span," Opt. Express **15**(12), 7677–7681 (2007).
36. P.-G. De Gennes, F. Brochard-Wyart, and D. Quéré, *Capillarity and wetting phenomena: drops, bubbles, pearls, waves* (Springer Science & Business Media, 2004).
37. B. Carroll, "The accurate measurement of contact angle, phase contact areas, drop volume, and Laplace excess pressure in drop-on-fiber systems," J. Colloid Interface Sci. **57**(3), 488–495 (1976).
38. M. Gorodetsky, "Optical microresonators with gigantic quality factor," Moscow, Fizmatlit (2011).
39. C. Lam, P. T. Leung, and K. Young, "Explicit asymptotic formulas for the positions, widths, and strengths of resonances in Mie scattering," J. Opt. Soc. Am. B **9**(9), 1585–1592 (1992).
40. M. Oxborrow, "How to simulate the whispering-gallery modes of dielectric microresonators in FEMLAB/COMSOL," in *Lasers and Applications in Science and Engineering*, (International Society for Optics and Photonics, 2007), 64520J–64520J–64512.

1. Introduction

An optical whispering-gallery resonator [1] confines circulating light by total internal reflection on its spheroidal interface. This boundary must therefore border between an internal high refractive-index region and an external low refractive-index region. The spheroid interface can be a solid-gas interface [2–4], a solid-liquid [5, 6], a liquid-gas [7–13], or a liquid-liquid one [14–16].

In this paper we will focus on liquid-liquid micro-resonators. Liquid resonators are easy to fabricate. They are exceptionally smooth, and therefore minimize scattering losses. Recently, liquid resonators were miniaturized and fiber coupled [9, 12, 16], making them attractive for various applications and fundamental studies. Liquid resonators enable

phenomena that cannot occur in solid ones, including the propagation of capillary waves [11]. A liquid resonator can therefore function as a multisensory detector relying on acoustical [13], capillary [11] and optical modes.

Liquid droplets can be used as sensors in two different ways. Firstly, the analyte can be absorbed on its surface similar to the case of solid resonators [17–23], and be detected by the analyte-induced changes in the spectra of WGM. Different WGM will be affected by the analyte differently, and by comparing spectral responses of different modes to the analyte one can, in principle, be able to determine both the size and position of the analyte following the ideas put forward in [23]. Since the shape of a liquid drop on a fiber studied in this work is different from almost spherical resonators considered in [23] and other papers on solid resonators, the exact dependence of the spectral shifts on the analyte's size, position and the parameters of the WGMs will differ from those presented in [23] and elsewhere. Generalization of the ideas of reference [23] to the system studied here will require special consideration, lying outside of the scope of this paper.

Secondly, analytes can be encapsulated by the resonators (this regime is not possible in solid resonators), in which case analytes are expected to be pulled toward the region of strongest electric field resulting in improved sensitivity.

However, before one can consider any possible applications of the liquid droplet-on-the-fiber resonators, the first necessary step must be to study the spatial structure of the WGMs in these structures, and to develop means of identifying them. This task, which is the main objective of this paper, is best achieved by spatial mapping of the modes accompanied by comparison of experimental results with those of numerical simulations. One of the interesting unexpected results of our study with important implications for many future applications of these resonators is the presence of multiple mode crossing. While this phenomenon was also previously observed in solid resonators [24, 25], its manifestations are shape-specific and require special consideration in each particular case. Since level-crossings affect identification of the modes, the study of this effect undertaken in this paper is particularly important.

Droplet micro-resonators [12, 16] can be continuously pumped while light interacts with their acoustical [13] and capillary [26, 27] modes. In this regard, the structure of their optical modes, that are studied here, helped us in understanding the opto-acoustical [13] and opto-capillary interactions [26, 27] in the droplets. For example, high-order optical modes are expected to well overlap (and consequently well interact) with high-order mechanical- and capillary-mode as we indeed observed.

The eigenfunctions of an optical whispering-gallery mode can be indexed by 3 quantum numbers: n, l, and m, which represent the radial, polar, and azimuthal modal-order. The circulation direction is given by the sign of m: positive for clockwise circulating mode and negative for counter clockwise circulating mode. As will be shown below, more than half of the modes in our droplet resonator have a "sibling" at a distance smaller than the resonance linewidth. As a result, we can pump two co-circulating modes with different n, l, m indices, with a single-frequency laser [24, 25].

Such pairs of modes typically exhibit various interference patterns along the circulation direction of light. The interference pattern does not move since its group velocity, $\delta\omega/\delta k$, is zero. Therefore, the pattern can be referred to as "stopped light" [24]. In a sphere, these degenerated modes were viewed as a standing zigzag patterns along the equator [24], made by the interference between the two modes. In a toroid, such degenerated modes gave rise to a standing flower-shape interference [25]. In this flower shape, the number of petals along the azimuthal direction describes the m difference and the number of petal-circles describes the n difference.

The phenomenon is called "level-crossing" [25] since the frequencies of the modes will typically cross each other upon changing one of the parameters (e.g. refractive index). Level-

crossing can be avoided (mode veering) when the modes differ only by their n, l indices and non-avoided when m also differs, as explained in more details in [25]. Due to the large transverse cross-section of the droplet, there are more high-transverse-order modes than, for example, in a toroid, and therefore an abundance of level crossings are expected.

Degeneracy between clockwise and counterclockwise modes is removed in the presence of nanoparticles [28–30], which may manifest experimentally either as mode splitting [31], or, if the splitting is as smaller than the width of the modes, as a frequency shift [5]. Additional degeneracy due to level-crossing is expected to enhance this effect, and enhance the sensitivity of detection. The expected increase in the sensitivity due to level-crossing effects is based upon the following arguments. In the absence of the mode crossing effects there are just two degenerate counter-propagating modes interacting with the analyte and responsible for all the observed spectral effects. When the level-crossing occurs, the number of modes interacting with the analyte increases, resulting in the respective increase of the electric field polarizing the analyte. It is not surprising, therefore, to expect proportional enhancement of the analyte-related spectral effects. The extreme case of the increased degree of degeneracy occurs in ideally spherical resonators, where instead of just two modes, the analyte interacts with $2l + 1$ modes. It was shown in Ref [28]. that transition from spheroidal to spherical resonators results in an increase of the analyte-induced spectral shifts of WGM by the factor roughly proportional to l.

2. Experimental setup

We fabricate our resonator by dipping a silica cylinder in silicon oil with a refractive index of 1.4036. When the cylinder is taken out of the oil, a droplet is attached to its end. Fusing the extremity of the cylinder into a microsphere helps in pinning the droplet at the end of the cylinder while prohibiting its axial motion.
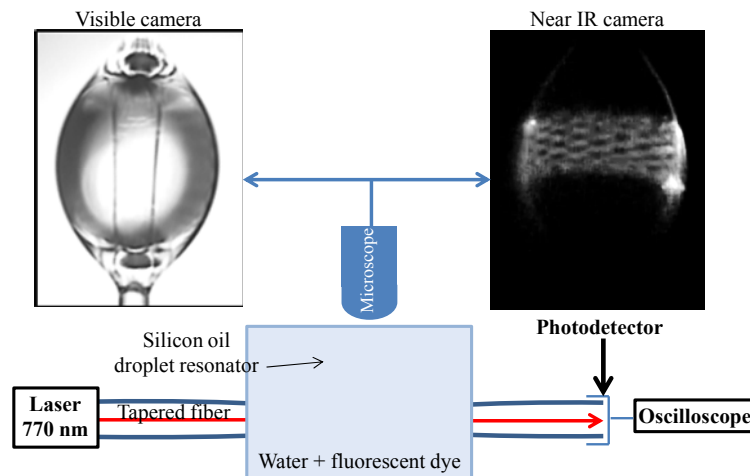

Fig. 1. Experimental setup. The light is coupled from a tapered fiber to circumferentially circulate in a microdroplet resonator. The tapered fiber and the resonator are placed in a solution of fluorescent dye in water, which allows us to see the modes in the droplet using a near IR camera.

As one can see in Fig. 1, our experimental setup includes a micro-droplet resonator (120 µm) and its aquatic surrounding. The water environment contains a 3 µmol/L solution of ADS780WS fluorescent dye. This fluorescent material absorbs light at the wavelength of the optical mode (770 nm) and incoherently emits at 810 nm. The emission from the fluorescent material will be used to map the optical mode. A filter is placed between the camera and the microscope to block any scattered light from the laser, and to selectively transmit the light

emitted from the excited dye's molecules. The advantage of the fluorescent mode mapping technique [24, 25] is that incoherent light can be imaged at high resolution (when compared to coherent light). In addition, the fluorescent light emerges from the thin evanescent region only, and therefore can be easily contained within the microscope depth-of-focus.

Optical coupling of the light into the cavity is performed via a tapered fiber [32–35]. A Q of 10^6 was measured trough the resonance linewidth while the droplet is immersed in dye-doped water. This Q is 3.8 times lower when compared to what is expected from the measured liquid absorption of $\alpha = 0.5\,m^{-1}$ (measured using a spectrophotometer (Cary 5000 UV-Vis-NIR)). Such a reduction in Q is common while immersing resonators in liquid.

3. Experimental results

We couple light inside the resonator, and scan the laser's emission wavelength from 770 nm to 780 nm. Using the near IR camera, we record the shape of the modes while the laser is swept through them (see Supplementary material).
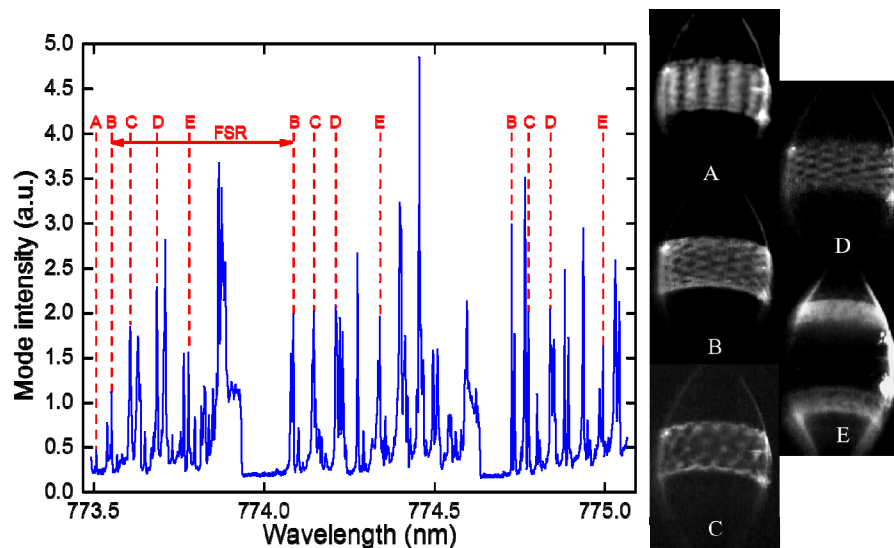

Fig. 2. Experimental results. We show the mode intensity as measured from the fluorescent emission versus laser's wavelength. Modes B-E repeats themselves every free spectral range. (see Visualization 1 in supplemental material for the movie of the optical modes)

As typical to such resonators [24, 25], two shapes of resonances were seen. In more details, throughout the scan we observe both single modes, as in Fig. 2(E), and level-crossings, as in Fig. 2(A)-2(D), representing spectrally-overlapping pairs of modes. Surprisingly, we notice that about 80% of the modes have an overlapping sibling. The spatial patterns in Fig. 2(A)-2(D) have 12, 10, 14, and 8 nodes along their circumference. This number of nodes suggests that these mode pairs have azimuthal number (m_1, m_2) where $|m_1 - m_2| = 12, 10, 14$, and 8.

Figure 2(B) represents a level-crossed pair for which the difference in the azimuthal order is 10. This very-same resonance structure repeats itself 3 times in wavelength intervals of 0.6 nm. Similarly, the structure photographed in Fig. 2(C) is appearing 3 times at 0.6 nm intervals. All in all, we have 4 resonance structures in Fig. 2(B)-2(E), each of them appears 3 times at a spectral location that is far by an integer multiplication of 0.6 nm from their first appearance. Calculating the free spectral range (FSR) from the size of our resonator suggests that it is 0.59 ± 0.01 nm. We might therefore conclude that level crossing between modes of

azimuthal orders (m_1, m_2) will tend to repeat at ($m_1 + 1$, $m_2 + 1$). Still, this is not always true as one can see in resonance in Fig. 2(A) that appears only once.

4. Theory and modeling of experimental results

In order to verify that experimentally observed patterns indeed correspond to crossing modes and to assist with mode identification we carried out numerical simulations of the mode in the droplet using finite-element method FEM realized in COMSOL complimented with approximate analytical estimates. To carry out the simulations we first need to model the shape of the droplet. Using the equilibrium condition for the droplet surface [36] in the form

$$\frac{1}{r_1} + \frac{1}{r_2} = \frac{\Delta p}{\gamma}, \tag{1}$$

where r_1, r_2 are the principal radii of curvature, Δp is the pressure difference across the fluid interface, and γ is the surface tension, one can find an explicit analytical shape form the droplet profile [37].
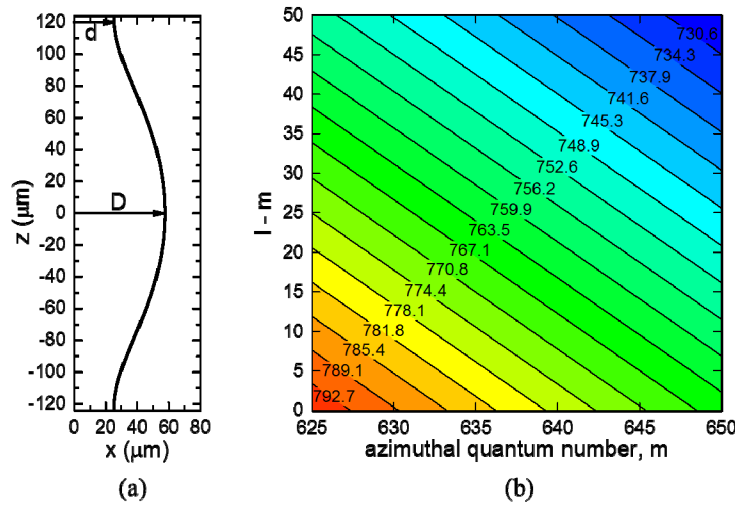

Fig. 3. (a) Profile of the droplet with equatorial radius D on the fiber with radius d. (b) A level plot of Eq. (6) corresponding to different first radial order TE resonances with wavelengths expressed in nm. One can see that multiple resonances with different values of orbital and polar numbers can appear at the chosen frequency within some linewidth.

Using a cylindrical coordinate system with its polar axis Z along the axis of symmetry of the droplet (see Fig. 3(a)) the cross-section of the droplet in the X-Z plane can be presented in the form of elliptical integrals $\mathrm{F}(\varphi, k)$ and $\mathrm{E}(\varphi, k)$ of the first and second order respectively:

$$z = \pm \left[ad\,\mathrm{F}(\varphi, k) + D\,\mathrm{E}(\varphi, k) \right]. \tag{2}$$

Here d and D are radius of the fiber and the equatorial radius of the droplet, parameter a depends on the contact angle θ as

$$a = \frac{D\cos\theta - d}{D - d\cos\theta}, \tag{3}$$

while the argument φ of the elliptic integrals is related to the coordinate x of the point on the droplet surface according to

$$x^2 = D^2 \left(1 - k^2 \sin^2 \varphi\right) \tag{4}$$

with k defined as $k^2 = 1 - a^2 d^2 / D^2$. The equatorial plane of the droplet corresponds to $\varphi = 0$ and, obviously, $x = D$. In the vicinity of the equatorial plane, the surface of the droplet can be approximated by a spheroid, in which case Eq. (2) must reduce to that of an ellipse. Indeed, considering limit $\varphi \ll 1$, we can bring this equation to the form

$$z = \pm \frac{ad + D}{D} \sqrt{D^2 - x^2}, \tag{5}$$

which describes ellipse with large and small semiaxes $R_1 = ad + D$ and $R_2 = D$, respectively, and ellipticity parameter $e = D / (ad + D)$. Using $D = 57.5\,\mu m$, $d = 25\,\mu m$ and $a = 1$, we find that $e = 0.7$. Fitting numerically Eq. (2) by an ellipse, we find a better approximation for the parameters of the effective spheroid with $R_1 = 91.3\,\mu$m and $e = 0.63$. Assuming that the WGMs excited in our experiments do not deviate too far from the equatorial plane, we can estimate their frequencies by combining the spheroidal approximation with the asymptotic expression obtained in the geometrical optics limit. Following [38], we can present them in the form

$$
\begin{aligned}
n_r k_{l,m,n} R_1 = {} & m - \alpha_n \left(\frac{m}{2}\right)^{1/3} + \frac{(2l - 2m + 1)R_1}{2R_2} - \frac{P n_r}{\sqrt{n_r^2 - n_0^2}} + \frac{3\alpha_n^2}{20}\left(\frac{m}{2}\right)^{-1/3} - \\
& \frac{\alpha_n}{12}\left[\frac{(2l - 2m + 1)R_1^3}{R_2^3} + \frac{2n_r^3 P\left(2P^2 - 3\right)}{\left(n_r^2 - n_0^2\right)^{3/2}}\right]\left(\frac{m}{2}\right)^{-2/3},
\end{aligned}
\tag{6}
$$

where $k_{l,m,n} = \omega_{l,m,n} / c$ is the vacuum wave number corresponding to WGM with frequency $\omega_{l,m,n}$, n_r and n_0 are the refractive indices of the resonator and surrounding medium respectively, α_n is the n-th zero of the Airy function defining the radial behavior of the mode. Parameter P is equal to unity for TE modes and $P = \left(n_0 / n_r\right)^2$ for TM modes. In the case of spherical resonators ($R_1 = R_2$) the dependence of these frequencies on the azimuthal number m vanishes and one reproduces well-known asymptotic formulas first derived in [39]. In order to illustrate the ubiquitous nature of the level crossings in non-spherical resonators we plot a level plot of Eq. (6) for TE modes of the first radial order close to the experimentally found resonances. One can see from Fig. 3(b) that multiple resonances with different values of the polar and azimuthal numbers can appear at almost the same frequency resulting in the level crossing phenomenon.

Using the analytical results as a starting point we also carried out accurate FEM simulation of the resonances using Eq. (2) to describe the shape of the drop and COMSOL Multiphysics computational platform to calculate frequencies, electromagnetic field patterns and other properties of WGMs excited in the drop. Due to the presence of the axisymmetric and reflection symmetries, simulations were limited to the 2D domain and, moreover, only half of the profile ($z \geq 0$) shown on Fig. 3(a) was used, surrounded by the correct set of the boundary conditions around the narrow region of WGM volume existing close to the surface of the drop. More details and specifics can be found, for example, in [40] and references therein, which uses "weak-form" expressions to analyze WGMs of dielectric microresonators. Numerical data from simulations with the wide range of values of m and within the spectral range under interest was exported to Matlab for further analysis and visualization. This way we were able to select pairs of WGMs satisfying imposed conditions

based on the experimental data. They include, but not limited to: change of m (which defines the number of fringes in azimuthal direction), spectral distance between modes' frequencies, vertical apparent size of the patterns, and so on. A couple of the results of the selection can be seen on Fig. 4, showing the normalized intensity of a single high-order mode (a) and the intensity of the sum of two level-crossed normalized modes (b) taken from the close vicinity to the exterior side of the drop.
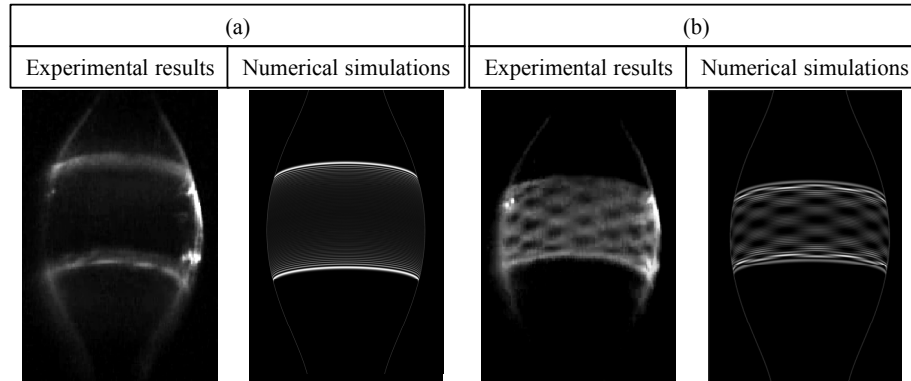

Fig. 4. Experimental results and simulations for (a) a high-order mode, similar to the ($n = 1$, $m = 588$, $l = 679$) mode, and (b) a level-crossed pair, similar to the interference between ($n = 2$, $m = 602$, $l = 653$) and ($n = 2$, $m = 610$, $l = 649$) modes. Numerical results were outlined to show profile of the drop.

In more details, Fig. 4(a) depicts a mode shape that is rotational symmetric along the axial direction. Our analysis shows that this mode is similar to the ($n = 1$, $m = 588$, $l = 679$) mode. Contrary to this mode shape, the mode in Fig. 4(b) exhibits a zigzag pattern along the azimuthal direction. It is not rotational symmetrical, yet rotation by 360/8 degrees does not change the pattern. Our analysis shows that this shape is typical to the interference between ($n = 2$, $m = 602$, $l = 653$) and ($n = 2$, $m = 610$, $l = 649$) modes that have a sufficiently close resonance frequency yet a different m number. As mentioned, the 8 fringes along the azimuthal direction represent the m numbers' difference.

5. Conclusion

Experimentally mapping the resonances of a liquid micro-resonator revealed that most of the droplet's modes have a sibling at a frequency distance that is comparable to their linewidth. The interference between such mode-pairs produces various standing patterns which are called level-crossing. We also carried out numerical simulations of WGM in this system with COMSOL, using an analytical expression derived from Laplace's formula [36, 37] to describe the drop's shape. Simulations showed that the studied system possesses a large number of spectrally close modes that can produce a whole gallery of various interference patterns. On one hand, the ubiquitous nature of this effect presents a very interesting opportunity for studying various types of level-crossing phenomena, but on the other hand, makes unambiguous identification of the participating modes more difficult. The crossing modes and their expected split upon the introduction of an analyte can be used to increase sensitivity of biosensors based on WGM resonators.

Acknowledgments